

PAPER

Diffractive optics for axial intensity shaping of Bessel beams

To cite this article: Raghu Dharmavarapu *et al* 2018 *J. Opt.* **20** 085606

View the [article online](#) for updates and enhancements.

Related content

- [Shaping the on-axis intensity profile of generalized Bessel beams by iterative optimization methods](#)
Runze Li, Xianghua Yu, Tong Peng et al.
- [Annular-aperture diffractive axicons illuminated by Gaussian beams](#)
Jixiong Pu, Huihua Zhang, Shojiro Nemoto et al.
- [Shape invariant higher-order Bessel-like beams carrying orbital angular momentum](#)
Y Ismail, N Khilo, V Belyi et al.





IOP | ebooks™

Bringing you innovative digital publishing with leading voices to create your essential collection of books in STEM research.

Start exploring the collection - download the first chapter of every title for free.

Diffractive optics for axial intensity shaping of Bessel beams

Raghu Dharmavarapu^{1,2,3} , Shanti Bhattacharya² and Saulius Juodkazis^{1,3} 

¹ Centre for Micro-Photonics, Faculty of Science, Engineering and Technology, Swinburne University of Technology, Hawthorn VIC 3122, Australia

² Centre for NEMS and Nanophotonics (CNNP), Department of Electrical Engineering, Indian Institute of Technology Madras, Chennai 600036, India

³ Melbourne Centre for Nanofabrication, the Victorian Node of the Australian National Fabrication Facility, 151 Wellington Rd., Clayton 3168 VIC, Australia

E-mail: raghu.d@ee.itm.ac.in

Received 20 March 2018, revised 24 June 2018

Accepted for publication 5 July 2018

Published 17 July 2018



CrossMark

Abstract

Bessel beams (BBs) appear to be immune to diffraction over finite propagation distances due to the conical nature of light propagation along the optical axis. This offers promising advantages in laser fabrication. However, BBs exhibit a significant intensity variation along the direction of propagation. We present a simple technique to engineer the axial intensity of the BBs over centimeter-long propagation distances without expansion of the incoming laser beam. This method uses two diffractive optical elements (DOEs), one converts the input Gaussian intensity profile to an intermediate intensity distribution, which illuminates the second DOE, a binary axicon. BBs of a desired axial intensity distribution over a few centimeters length can be generated.

Keywords: diffractive optics, beam shaping, bessel beams

(Some figures may appear in colour only in the online journal)

1. Introduction

Bessel beams (BBs) have an elongated axial light intensity distribution that is immune to diffraction over finite propagation distances. The analytical expression of the BBs intensity [1] was refined in [2], where it was demonstrated that the zeroth order BB is a member of a special class of solutions to the Helmholtz equation that are propagation invariant.

The transverse intensity profile of the BBs follows a zeroth order Bessel function, which has a high intensity central peak surrounded by number of concentric rings. Unlike a traditional Gaussian beam, whose beam waist diverges, the transverse intensity profile of the BB remains unchanged as it propagates. The ideal BB with rings extending infinitely in the radial direction maintains constant axial intensity (with an infinite amount of energy). Therefore, only radially truncated approximations of BBs are practically realizable. BBs also exhibit another interesting property known as self-healing, i.e. the ability of the beam to reconstruct after encountering an obstacle. Owing to these special

properties, these beams are being used as an alternative to Gaussian beams in many applications such as optical manipulation [3], high precision hole drilling [4] and light sheet microscopy [5]. Several techniques have been proposed to generate these beams: refractive axicons [6], diffractive axicons [7] and annular apertures [8].

Even though the above mentioned techniques can be used to generate Bessel-like beams, they all suffer from non-uniformity of intensity along the axis. The axial intensity variations along the axis limits the applicability of these beams. Several techniques have already been reported to create BBs with specific axial intensity profiles [9, 10]. An axicon with an annular aperture and a logarithmic phase profile has been proposed to flatten [11] the axial intensity of the Bessel-like beams. Lens axicons [12] were proposed to generate uniform axial intensity BBs over long propagation distances, but this method uses an annular aperture, which results in blockage of light and hence, has low efficiency. It was shown that by superposing a finite number of BBs with different longitudinal wave numbers, one can produce arbitrary desired axial intensities known as

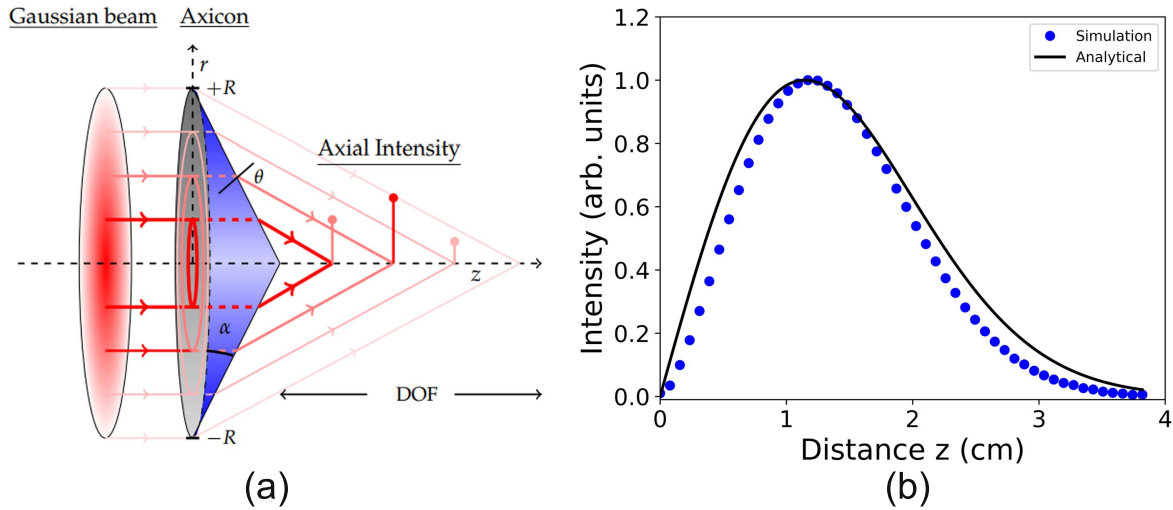


Figure 1. (a) Refractive axicon ray tracing for the Gaussian input; DOF is the depth of focus. (b) Analytical (line) and Fresnel integral simulated (dots) axial intensity of the Bessel beam generated by an axicon with radius $R = 2$ mm, $\alpha = 1.6^\circ$ for an incident Gaussian beam of waist 0.5 mm.

‘frozen waves’ (FW) [13]. Tracio *et al* used the FW approach and experimentally realized a BB using a holographic technique [14, 15]. Controlling axial intensity was also achieved in absorbing fluids to counter the propagation losses [16, 17]. Recently cardioid-like apertures [18] were proposed to flatten the axial intensity oscillations. The authors have shown the simulation results of the axial intensity of an ideal zeroth order BB propagating through a cardioid-like aperture. Large apertures of radius 50 mm were used to achieve long propagation distance of 30 m. In this paper, we have experimentally shown long propagation distances for a relatively very small axicon radius of 1 mm.

For emerging industrial applications, such as laser dicing, drilling and inscription of optical elements, the two important requirements are the ability to control the beam intensity along the axis and to move the focus [19]. In order to use BBs for material modification [20, 21], it is preferable to have simple optical elements, which can be directly inserted in the path of a laser’s Gaussian-like beam to generate BBs. In this paper, we demonstrate a technique that uses two diffractive optical elements (DOEs). The first DOE converts the incident Gaussian beam into an intermediate intensity distribution, which illuminates the second DOE, a diffractive axicon to produce the desired on-axis intensity. In this manner, the final axial intensity can be engineered to have any desired variation by suitably adjusting the intensity output of the first DOE. This is demonstrated with examples of axial intensity distributions that are: (i) linearly increasing, (ii) uniform, and (iii) exponentially increasing. DOEs were designed for each case, and the axial intensity outputs were simulated. Simulation results were compared with experimental results for the first case. The DOEs were fabricated using electron beam lithography (EBL) and the desired on-axis intensity profiles were achieved over long propagation distances of a few centimeters.

2. Theory: BB

Axicons—conical lenses—are optical elements that have rotational symmetry about the z -axis (figure 1(a)). They generate a quasi-BB throughout their depth of focus (DOF) region. Beyond the DOF, the beam gradually transforms into a ring of constant width with increasing radius as it propagates. The important parameters that characterize an axicon are its front face radius, R , the cone angle, α , and the refractive index, n . These parameters together determine the length of the DOF of the axicon. The scalar equation of a zeroth order BB propagating in the z direction can be described in cylindrical coordinates by:

$$E(r, \phi, z) = A \cdot \exp(ik_z z) \cdot J_0(k_r r), \quad (1)$$

where A is the amplitude, k_z and k_r are the longitudinal and transverse wave numbers that satisfy the equation $k = \frac{2\pi}{\lambda} = \sqrt{k_z^2 + k_r^2}$ and λ is the wavelength.

The numerical aperture (NA) of an axicon is a function of the cone angle α as:

$$NA = \sin(\theta) = \sin(\sin^{-1}(n \cdot \sin(\alpha)) - \alpha). \quad (2)$$

The full width half maximum (FWHM) of the zeroth order BB can be derived from equation (1) as:

$$FWHM = \frac{2.25}{k_r} = \frac{0.358\lambda}{NA}. \quad (3)$$

Consider the input light beam to be a collection of rays traveling parallel to the z -axis. All these rays refract at the conical surface of the axicon towards the axis with the same angle θ . All the rays at one radial distance, come to focus at one point on the axis. The rays incident at the extreme of the axicon (i.e. the furthest radial distance) determine the DOF of the axicon, as shown in figure 1(a). Using Snell’s law, $\sin \theta = n \sin \alpha$ and applying the small angle approximation

for α , the DOF is found to be:

$$\text{DOF} = \frac{w}{(n-1)\alpha}, \quad (4)$$

where w is the radius of the illuminating beam. Even though the axicon generates a BB, the intensity along the axis is not uniform within the DOF. To demonstrate this, we consider a standard Gaussian intensity profile for the incident beam, i.e.

$$I_{in}(r) = I_0 \exp\left(\frac{-2r^2}{w_0^2}\right), \quad (5)$$

where w_0 is the beam waist (radius), I_0 is the peak intensity of the Gaussian beam and $r = \sqrt{x^2 + y^2}$ is the radial distance from the z -axis. To derive an analytical expression for the on-axis intensity, we consider a thin annular ring of width dr , inner radius r and outer radius $r + dr$ on the front surface of the axicon. The amount of power passing through this annular ring is given by:

$$\begin{aligned} P_{ring}(r) &= I_0 \exp\left(\frac{-2r^2}{w_0^2}\right) [\pi(r+dr)^2 - \pi r^2] \\ &\approx I_0 \exp\left(\frac{-2r^2}{w_0^2}\right) 2\pi r dr. \end{aligned} \quad (6)$$

From the geometrical law of energy conservation, this power $P_{ring}(r)$ gets spread out along a length dz on the z -axis. Therefore, the axial intensity is given by $AI(z) = P_{ring}(r)/dz$. Dividing both sides of equation (6) with dz and substituting $r = z(n-1)\alpha$ from equation (4) gives:

$$AI(z) = I_0 \exp\left(\frac{-2z^2(n-1)^2\alpha^2}{w_0^2}\right) 2\pi z(n-1)^2\alpha^2. \quad (7)$$

From equation (7), it can be seen that the on-axis intensity of a BB generated using an axicon is directly related to the input intensity profile $I_{in}(r)$. Equation (7) can be generalized and the input intensity profile $I_{in}(r)$ can be written in terms of AI as:

$$I_{in}(r) = MAI[z = r/(n-1)\alpha]/r, \quad (8)$$

where $M = 1/2\pi(n-1)\alpha$ is a constant for the designed axicon. It should be noted that equation (8) should be used to compute the on-axis intensity only for $0 < z < \text{DOF}$.

To confirm the validity of this equation, we have compared the axial intensity derived from equation (8) with the Fresnel simulations of a diffractive axicon for a Gaussian input shown in figure 1(b). The axicon (DOE2) parameters used were: $R = 1$ mm and $\alpha = 1.6^\circ$, and the illuminating Gaussian beam waist radius was 0.5 mm, these parameters result in a DOF of ≈ 3.5 cm, which is useful for practical applications. Simulated results are in good agreement with analytical calculations.

3. Samples and fabrication

The DOEs were designed with a diameter of 2 mm operating at a wavelength of 633 nm and their phase profiles were quantized to 0 and π for fabrication feasibility with EBL.

Polymethylmethacrylate resist 950 K A8 (MicroChem GmbH) was used as the EBL resist. Indium tin oxide (ITO) coated glass plate was used as a substrate. The ITO layer prevents charging during EBL writing. Presence of the ITO layer decreased the transmission to 85% for 633 nm. The EBL parameters were as follows: acceleration voltage 10 kV, aperture $30 \mu\text{m}$ and dose $70 \mu\text{C cm}^{-2}$. The DOEs were developed in a mixture of methyl isobutyl ketone and isopropyl alcohol (IPA) at ratio 1:3 for 50 s followed by cleaning in IPA for 30 s.

4. Results and discussion

For an axicon, the on-axis intensity rises to a peak and gradually declines towards the end of the DOF (figure 1(b)), when the incident beam is Gaussian-like. Therefore, for example, when uniform axial intensity is desired, one can only utilize these beams over a very limited axial region, where the intensity might be considered uniform. Alternately, the beams could only be used in applications where uniformity is not important. The technique discussed in the following section allows one to engineer the axial intensity of BBs using two DOEs. The output is simulated by calculating the intensities at different planes along the beam propagation direction using the Fresnel diffraction integrals [22]. The DOEs were fabricated using EBL. With this method, desired on-axis intensity profiles were achieved over long propagation distances of a few centimeters.

4.1. Engineering the axial intensity

As it was shown in equation (8), the on-axis intensity is directly linked to the incident intensity profile. Therefore, this relationship can be used to back-calculate the input intensity $I_{in}(r)$ that gives the desired $AI(z)$. As most laser sources will have a Gaussian intensity profile, we need to design an optical element (DOE1) that converts the Gaussian intensity into the desired intermediate intensity $I_{in}(r)$ at the input plane of the diffractive axicon (DOE2). The phase profile of DOE1 is calculated using either the simplified mesh technique [23] or the Gechberg–Saxton (G–S) algorithm [24]. The following axial intensities are presented in the next section: (i) linearly increasing, (ii) uniform, and (iii) exponentially increasing.

4.1.1. Simulation: a linearly increasing axial intensity. For a linearly increasing axial intensity, the axial intensity is:

$$AI(z) = az, \quad (9)$$

where a is a positive constant. We get the desired input intensity for the diffractive axicon, by substituting this in equation (8):

$$I_{in}(r) = 2\pi a M^2, \quad (10)$$

i.e. a flat-top beam. Since the input and the desired output intensities are known, they can be used to calculate the phase distribution that would convert one to the other. While the G–S algorithm is perfect for such problems, it generates a

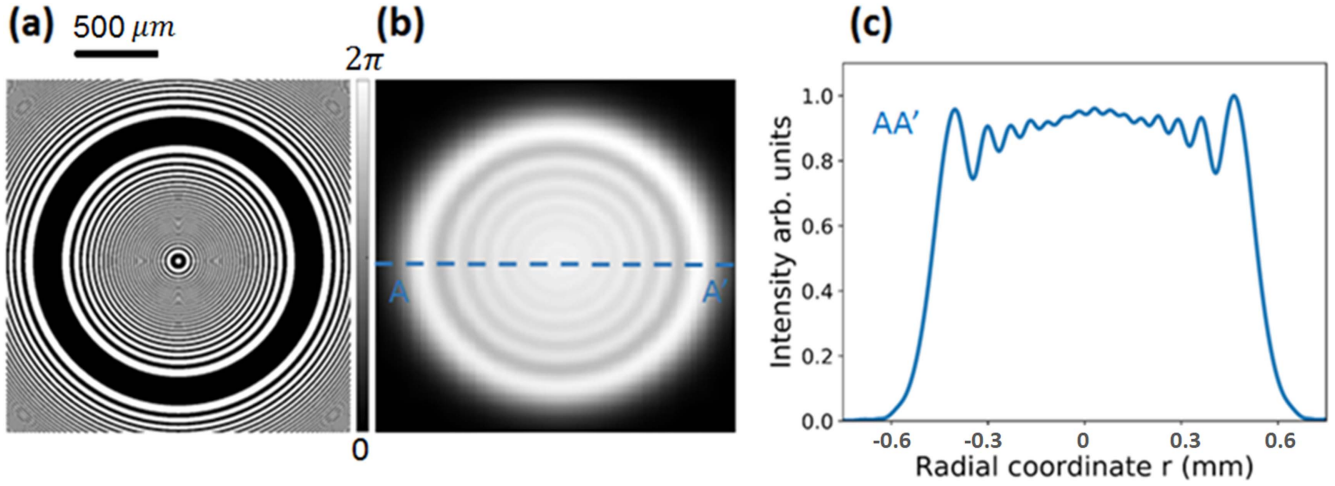


Figure 2. Simulation results. (a) Phase profile of DOE1, (b) intensity profile created at the front surface of the axicon, 10 cm behind the DOE1, (c) intensity profile along the central line AA' of (b).

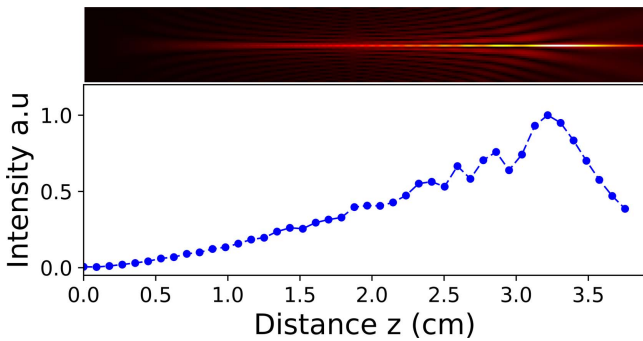


Figure 3. Fresnel simulation (same method as in figure 1) of linearly increasing axial intensity and beam cross section in the yz-plane.

random phase variation, which leads to scattering in practical systems. In order to avoid this, the calculated phase distribution should be continuous.

In the simplified mesh technique, the incident and output beams are each divided into a mesh consisting of zones of equal power. Eikonal equations [25] are used to connect the input to the output zones. The phase distribution $\phi(x, y)$, required to produce the desired output is obtained by solving these equations [23, 26].

Since the energy in each zone in the input plane is directed to a similarly located zone in the output plane and as the equations are solved simultaneously, the phase obtained is continuous. It should be pointed out that this technique is useful in cases, where the meshes are easy to construct.

In our simulations, the input Gaussian beam waist diameter was chosen as 1.1 mm to match the laser beam used in the experiment. For accurate simulation results, the phase distribution of DOE1 is quantized to 0 and π as shown in figure 2(a), which makes it a closer approximation to the fabricated DOE1. DOE1 creates a circular flat-top beam. Simulated $I_{in}(r)$ at the input of DOE2 and the on-axis intensity are shown in figures 2 and 3, respectively. The oscillations in the on-axis intensity can be attributed to the oscillations in the flat-top input, that arise due to the diffractive nature of the DOE1 and the axicon. These oscillations can be suppressed

by using multi-level/continuous phase diffractive elements, these also help to improve the efficiency of the generated BB.

4.1.2. Simulation: an uniform axial intensity. The uniform axial intensity is desired for many practical applications. The axial intensity in this case linearly increases to its maximum and stays uniform thereafter:

$$AI(z) = az \quad \text{for } 0 < z < d_1; \\ = a \quad \text{for } d_1 < z < \text{DOF}; \quad (11)$$

where a is a positive constant. The on-axis intensity is constant between the axial points d_1 and the DOF. The desired $I_{in}(r)$ to create this axial intensity is:

$$I_{in}(r) = aM \frac{1}{r}, \quad (12)$$

which is a hyperbolic intensity profile. A hyperbolic intensity profile has very high intensity close to the center as r approaches zero. To avoid this, we have added a finite constant intensity at the center of $I_{in}(r)$ as shown in figure 4(c). In this case, the phase profile $\phi(x, y)$ that transforms the input Gaussian beam into the desired intensity profile was computed using the G–S algorithm. This is because the mesh of the output beam was more complicated for this intensity distribution. The corresponding Fresnel simulations are shown in figure 4. Simulated on-axis intensity is presented in figure 5(a).

4.1.3. Simulation: a parabolic axial intensity. Finally, a parabolic axial intensity profile has been realized to prove the versatility of this method:

$$AI(z) = az^2, \quad (13)$$

where a is a positive constant. The desired $I_{in}(r)$ to get this axial intensity is,

$$I_{in}(r) = 4\pi^2 aM^3 r, \quad (14)$$

which is a radially increasing intensity distribution. The simulated axial intensity shown in figure 5(b) was obtained for Fresnel simulations of the DOE1 shown in figure 6.

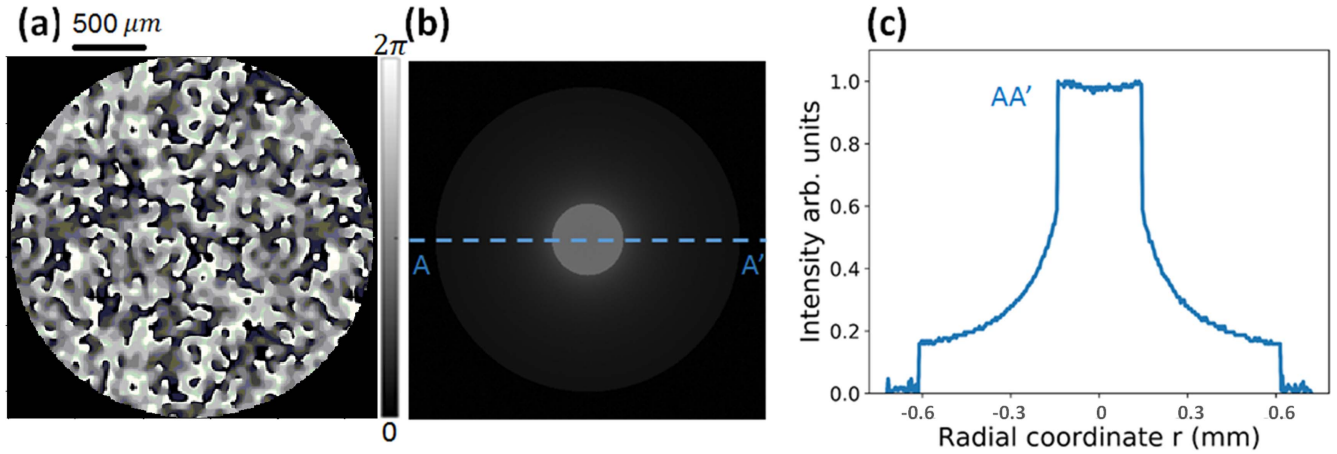


Figure 4. Simulation results. (a) Phase profile of DOE1 with random phase, which is a standard feature of a pure phase distribution generated by the G–S algorithm. This pattern is more complex to fabricate and it is more susceptible to scattering. (b) Intensity profile created at the front surface of axicon, 10 cm behind DOE1 (c) intensity profile along the central line AA' of (b).

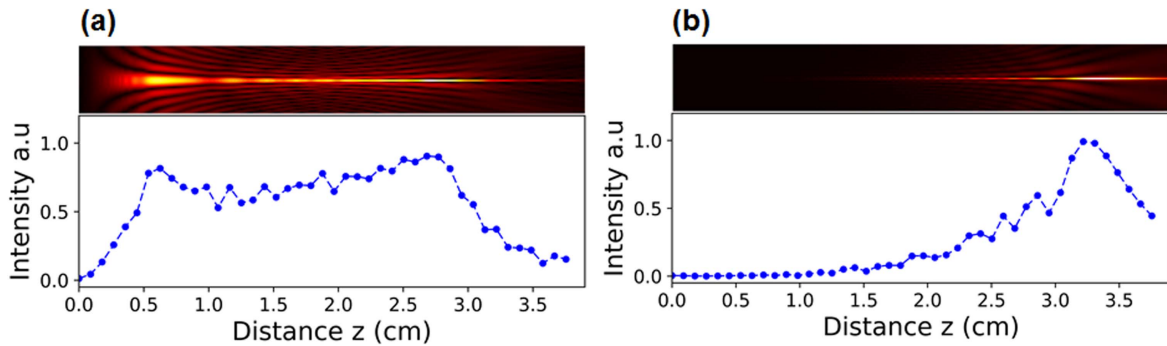


Figure 5. Fresnel simulation of the Bessel beam. (a) Uniform axial intensity, (b) parabolically increasing axial intensity with beam cross section in yz -plane shown above.

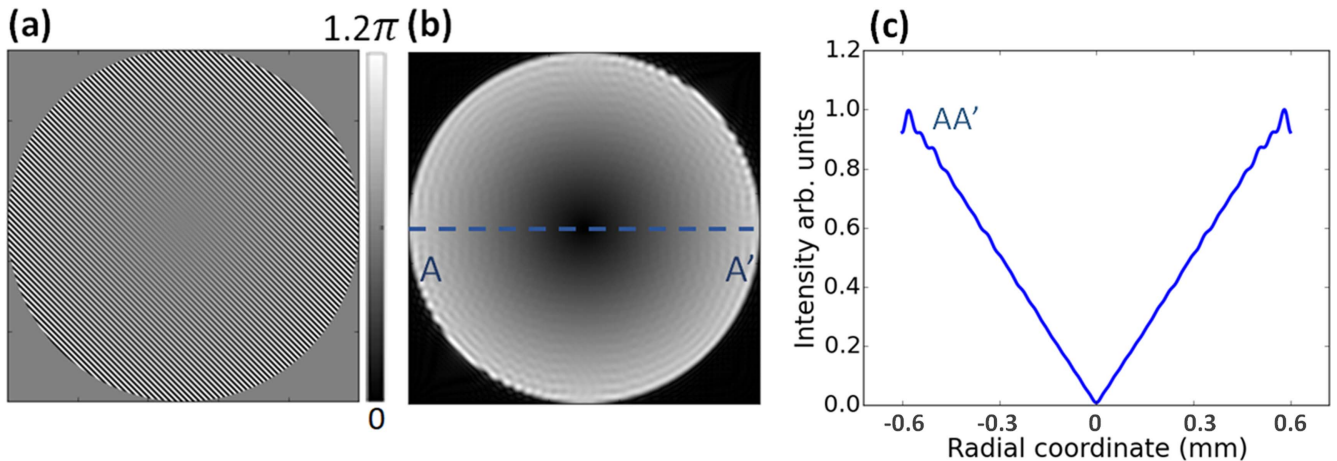


Figure 6. Simulation. The phase of DOE1 (a) and intensity (b) profiles created at the front surface of the axicon 10 cm behind the DOE1. The phase span in (a) is $0 - 2\pi$. (c) Intensity profile along the central line AA' shown in (b).

4.2. Fabricated BB generator

The experimental setup used for characterization of the fabricated optical elements is shown in figure 7(a). A collimated beam from a He–Ne source with $1/e^2$ diameter of 1.1 mm was passed through DOE1. This element was designed to create the desired $I_{in}(r)$ at the distance of 10 cm behind the

element, at the location of DOE2. Care has been taken to align the center of both DOE1 and DOE2. The confocal microscope images of the diffractive axicon and its profile are shown in figures 7(b) and (c).

Figure 8(a) shows the transverse intensity profile of the BB generated after DOE2, the FWHM is measured to be

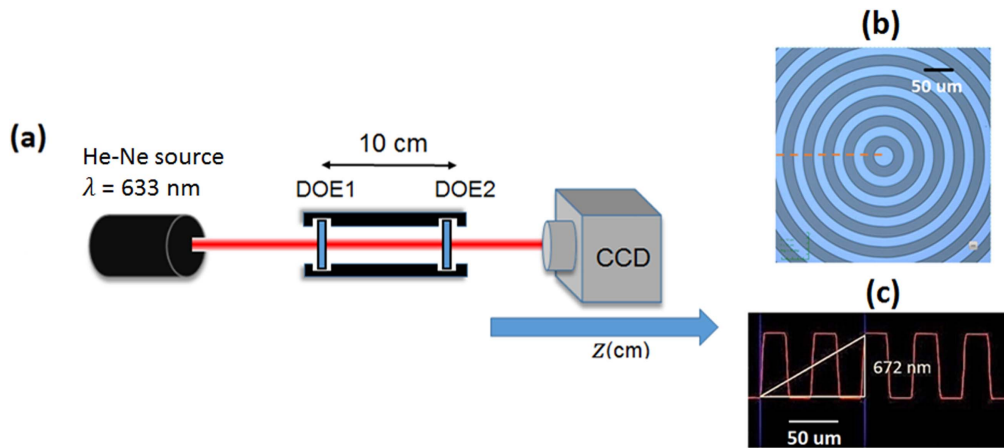


Figure 7. (a) Experimental setup, (b) microscope images of fabricated diffractive axicon designed for $R = 1$ mm and $\text{DOF} = 3.5$ cm. (c) Depth profile measured with confocal microscope.

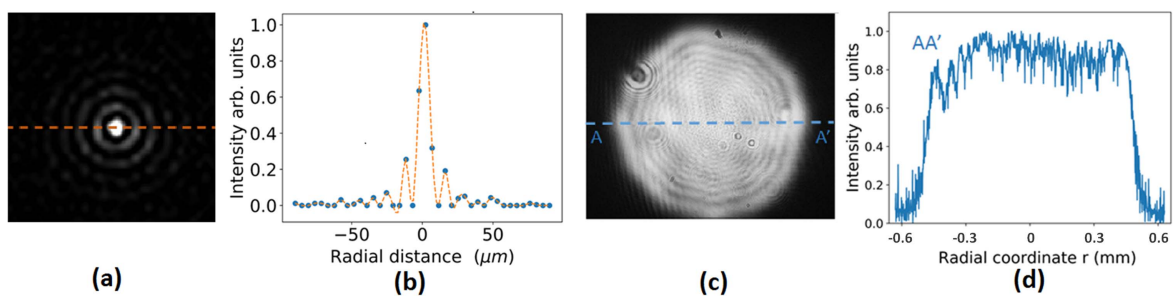


Figure 8. Experimental CCD images, (a) transverse intensity of Bessel beam after DOE 2 at $z = 3.2$ cm, (b) line profile along the center of (a) fitted to zeroth order Bessel function (dashed line) with an FWHM of $11 \mu\text{m}$, (c) flat-top intensity profile. (d) Intensity plotted along the central line of (c).

$\approx 11 \mu\text{m}$ which is close to the theoretical value of $15.52 \mu\text{m}$ for $\lambda = 633 \text{ nm}$ (equation (3)). The NA of the axicon was found to be 0.02, the low NA and large FWHM are the consequences of the long DOF. The on-axis intensity was measured by moving a CCD camera along the axis using a translation stage. The experimental results of the Gaussian to flat-top beam conversion with DOE1 are shown in figure 8(c). Measured values of the on-axis intensity for the Gaussian and flat-top incidence are summarized in figure 9(a).

The following procedure to analyse the BB property was implemented. The CCD-recorded transverse beam intensity profile was fitted with the cross section of the ideal 0th-order BB to align the centres of all the images captured along the DOF. The data were azimuthally averaged to its 1-dimensional central cross section and stacked to form the side view of the beam propagation as shown in figure 9(b). The beam cross section remained almost constant throughout the DOF. The axial intensity within the first 1.5 cm could not be measured as the CCD sensor housing had a depth of ≈ 1.5 cm within the C-mount. In this paper, we simulated three cases (linearly increasing, uniform along the axis and axially parabolic). The first and third cases were calculated using the mesh technique resulting in a continuous phase for DOE1. As both cases were calculated using the same method, only the first element was fabricated, using e-beam lithography. In order to do so, the analog phase was first binarised. The second case was calculated

using the GS algorithm, resulting in a random phase which is challenging to fabricate with EBL as it involves random and analog phase variations over small areas. Fabrication of spatially varying random phase patterns using metasurfaces can be achieved [27]. Capasso *et al* have recently demonstrated metasurface axicons [28] operating at visible wavelengths.

We used two binary DOEs written on ITO coated borosilicate glass substrate in tandem to achieve desired axial intensity profile. The theoretical maximum transmittance of each of these DOEs is 81% at the used wavelength of 632 nm which results in an overall efficiency of 65%. Further reduction in efficiency due to diffraction losses is a drawback of this technique as the DOEs are binary in nature. This situation can be improved by fabricating multi-level 3D DOEs using advanced fabrication techniques such as a grayscale EBL, scanning tip method for 3D structuring of resist, e.g. using NanoFrazor, or polymerization via direct laser writing [29]. Flat meta-optical elements [30] can also be used to fabricate these DOEs, which offer high resolution spatially varying phase that can minimize diffraction losses. Higher efficiencies could be achieved by depositing an anti-reflection coating on the DOEs. Since the purpose of DOE1 is only to generate an intermediate $I_{in}(r)$ for a predetermined axial intensity and is not essential for generation of the BB, the DOF ranging from a few millimeters-to-centimeters can be tuned just by changing DOE2.

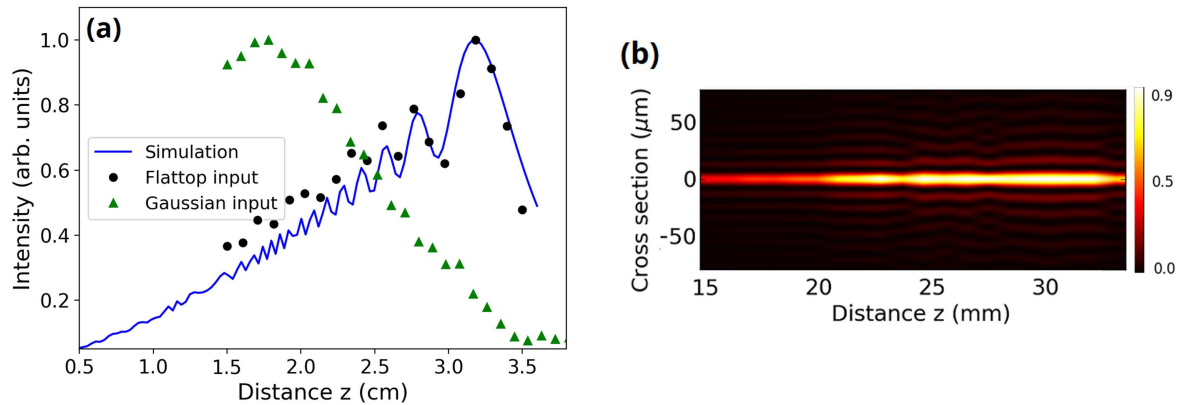


Figure 9. (a) On-axis intensity variation after DOE2. The solid line shows the simulated and dotted circles show the experimentally measured axial intensity when the flat-top beam was incident on DOE2. The dotted triangles curve shows the experimental results for an incident Gaussian beam. (b) Experimentally obtained data was fitted to ideal zeroth order Bessel beam and stacked to form the side view profile of the beam.

Typically, it is difficult to manufacture refractive axicons with cone angles less than $\sim 1^\circ$, which puts a limitation on the length of a few millimeters on the DOF. With the proposed technique, longer DOFs up to centimeters are possible as the diffractive axicons can be designed and easily fabricated for cone angles $< 1^\circ$. As this technique does not use any spatial light modulators for beam shaping, the two compact DOEs can be easily incorporated into any practical laser fabrication or imaging application that does not require real-time tuning of the axial intensity.

5. Conclusions and outlook

A simple method to engineer the axial intensity of the BBs, using two simple DOEs, over longer lengths 3.5 cm is demonstrated. This method is particularly advantageous over methods that use spatial light modulators, as those devices are expensive and difficult to include in industrial applications. We have designed DOEs to generate BBs with a linearly increasing axial intensity and with the uniform axial intensity. Experimental results show a good agreement with simulations.

One area of applications which can benefit from the presented simple design using flat optical elements is emerging in the field of free electron lasers where an optical excitation by ultra-short laser pulses should be combined coaxially with femtosecond x-ray beam which propagates on the center axis. By introducing center micro-hole in the DOE2 and a mirror with a hole between DOE1 and 2, it is possible to combine fs x-ray and optical beams to a small micro-focus with such folded geometry. A small central hole will not compromise an optical performance of the optical element.

Acknowledgments

The authors thank Center for NEMS and Nanophotonics (CNPN), IIT Madras for the use of their fabrication facilities.

Funding

Partial support via the Australian Research Council DP170100131 Discovery project.

ORCID iDs

Raghu Dharmavarapu  <https://orcid.org/0000-0002-8263-7966>

Saulius Juodkazis  <https://orcid.org/0000-0003-3542-3874>

References

- [1] Sheppard C and Wilson T 1978 Gaussian-beam theory of lenses with annular aperture *IEE J. Microw. Opt. Acoust.* **2** 105–12
- [2] Durmin J, Miceli J Jr and Eberly J 1987 Diffraction-free beams *Phys. Rev. Lett.* **58** 1499
- [3] Arlt J, Garces-Chavez V, Sibbett W and Dholakia K 2001 Optical micromanipulation using a Bessel light beam *Opt. Commun.* **197** 239–45
- [4] Matsuoka Y, Kizuka Y and Inoue T 2006 The characteristics of laser micro drilling using a Bessel beam *Appl. Phys. A* **84** 423–30
- [5] Planchon T A, Gao L, Milkie D E, Davidson M W, Galbraith J A, Galbraith C G and Betzig E 2011 Rapid three-dimensional isotropic imaging of living cells using Bessel beam plane illumination *Nat. Methods* **8** 417–23
- [6] McLeod J H 1954 The axicon: a new type of optical element *J. Opt. Soc. Am.* **44** 592–7
- [7] Dyson J 1958 Circular and spiral diffraction gratings *Proc. R. Soc. A* **248** 93–106
- [8] Airy G B 1841 I. On the diffraction of an annular aperture *Phil. Mag. J.* **18** 1–10
- [9] Cizmár T and Dholakia K 2009 Tunable Bessel light modes: engineering the axial propagation *Opt. Express* **17** 15558–70
- [10] Ouadghiri-Idrissi I, Giust R, Froehly L, Jacquot M, Furfaro L, Dudley J M and Courvoisier F 2016 Arbitrary shaping of on-axis amplitude of femtosecond Bessel beams with a single phase-only spatial light modulator *Opt. Express* **24** 11495–504

- [11] Jaroszewicz Z, Kołodziejczyk A, Staronski L R and Sochacki J 1993 Apodized annular-aperture logarithmic axicon: smoothness and uniformity of intensity distributions *Opt. Lett.* **18** 1893–5
- [12] Pu J, Zhang H and Nemoto S 2000 Lens axicons illuminated by Gaussian beams for generation of uniform-axial intensity Bessel fields *Opt. Eng.* **39** 803–7
- [13] Zamboni-Rached M 2004 Stationary optical wave fields with arbitrary longitudinal shape by superposing equal frequency Bessel beams: frozen waves *Opt. Express* **12** 4001–6
- [14] Vieira T A, Zamboni-Rached M and Gesualdi M R 2014 Modeling the spatial shape of nondiffracting beams: experimental generation of frozen waves via holographic method *Opt. Commun.* **315** 374–80
- [15] Vieira T A, Gesualdi M R and Zamboni-Rached M 2012 Frozen waves: experimental generation *Opt. Lett.* **37** 2034–6
- [16] Dorrah A H, Zamboni-Rached M and Mojahedi M 2016 Generating attenuation-resistant frozen waves in absorbing fluid *Opt. Lett.* **41** 3702–5
- [17] Schley R, Kaminer I, Greenfield E, Bekenstein R, Lumer Y and Segev M 2014 Loss-proof self-accelerating beams and their use in non-paraxial manipulation of particles' trajectories *Nat. Commun.* **5** 5189
- [18] Ye J-S, Xie L-J, Wang X-K, Feng S-F, Sun W-F and Zhang Y 2018 Flattening axial intensity oscillations of a diffracted Bessel beam through a cardioid-like hole *Opt. Express* **26** 1530–7
- [19] Shih A Y, Driscoll J D, Drew P J, Nishimura N, Schaffer C B and Kleinfeld D 2012 Two-photon microscopy as a tool to study blood flow and neurovascular coupling in the rodent brain *J. Cerebral Blood Flow Metab.* **32** 1277–309
- [20] Marcinkevičius A, Juodkazis S, Matsuo S, Mizeikis V and Misawa H 2001 Application of Bessel beams for microfabrication of dielectrics by femtosecond laser *Japan. J. Appl. Phys.* **40** L1197
- [21] Mikutis M, Kudrius T, Šlekys G, Paipulas D and Juodkazis S 2013 High 90% efficiency Bragg gratings formed in fused silica by femtosecond Gauss-Bessel laser beams *Opt. Mater. Express* **3** 1862–71
- [22] Goodman J W 2005 *Introduction to Fourier Optics* (Greenwood Village, CO: Roberts and Company)
- [23] Bhattacharya S 2008 Simplified mesh techniques for design of beam-shaping diffractive optical elements *Optik* **119** 321–8
- [24] Gerchberg R W 1972 A practical algorithm for the determination of the phase from image and diffraction plane pictures *Optik* **35** 237–46
- [25] Born M and Wolf E 1999 *Principles of Optics* ch 3 (New York: Elsevier)
- [26] Hermerschmidt A, Eichler H J, Teiwes S and Schwartz J 1998 Design of diffractive beam-shaping elements for non-uniform illumination waves *Proc. SPIE* **3291** 40–8
- [27] Dharmavarapu R, Ng S H, Bhattacharya S and Juodkazis S 2018 All-dielectric metasurface for wavefront control at terahertz frequencies *Nanophotonics Australasia 2017* vol 10456 (International Society for Optics and Photonics) 104561W
- [28] Chen W T, Khorasaninejad M, Zhu A Y, Oh J, Devlin R C, Zaidi A and Capasso F 2017 Generation of wavelength-independent subwavelength Bessel beams using metasurfaces *Light Sci. Appl.* **6** e16259
- [29] Wang X, Kuchmizhak A A, Brasselet E and Juodkazis S 2017 Dielectric geometric phase optical elements fabricated by femtosecond direct laser writing in photoresists *Appl. Phys. Lett.* **110** 181101
- [30] Khorasaninejad M and Capasso F 2017 Metalenses: versatile multifunctional photonic components *Science* **358** eaam8100